Life Metabolism, 2024, **3(6)**, loae025

https://doi.org/10.1093/lifemeta/loae025
Advance access publication 13 June 2024
Original Article

Immuno-electron microscopy localizes *Caenorhabditis elegans* vitellogenins along the classic exocytosis route

Chao Zhai[1,2,3], Nan Zhang[1,3], Xi-Xia Li[4], Xue-Ke Tan[4], Fei Sun[4,5,6,*], Meng-Qiu Dong[1,3,*]

[1]National Institute of Biological Sciences, Beijing 102206, China
[2]School of Life Sciences, Peking University, Beijing 100871, China
[3]Tsinghua Institute of Multidisciplinary Biomedical Research, Tsinghua University, Beijing 100084, China
[4]Center for Biological Imaging, Institute of Biophysics, Chinese Academy of Sciences, Beijing 100101, China
[5]National Key Laboratory of Biomacromolecules, CAS Center for Excellence in Biomacromolecules, Institute of Biophysics, Chinese Academy of Sciences, Beijing 100101, China
[6]University of Chinese Academy of Sciences, School of Life Science, Beijing 100049, China

[*]Corresponding authors. No. 15 Datun Road, Chaoyang District, Center for Biological Imaging, Institute of Biophysics, Chinese Academy of Sciences, Beijing 100101, China. E-mail: feisun@ibp.ac.cn (F.S.); No. 7 Science Park Road, Zhongguancun Life Science Park, National Institute of Biological Sciences, Beijing 102206, China. E-mail: dongmengqiu@nibs.ac.cn (M.Q.D.)

Abstract

Vitellogenins (VITs) are the most abundant proteins in adult hermaphrodite *Caenorhabditis elegans*. VITs are synthesized in the intestine, secreted to the pseudocoelom, matured into yolk proteins, and finally deposited in oocytes as nutrients for progeny development. How VITs are secreted out of the intestine remains unclear. Using immuno-electron microscopy (immuno-EM), we localize intestinal VITs along an exocytic pathway consisting of the rough endoplasmic reticulum (ER), the Golgi, and the lipid bilayer-bounded VIT vesicles (VVs). This suggests that the classic exocytotic pathway mediates the secretion of VITs from the intestine to the pseudocoelom. We also show that pseudocoelomic yolk patches (PYPs) are membrane-less and amorphous. The different VITs/yolk proteins are packed as a mixture into the above structures. The size of VVs can vary with the VIT levels and the age of the worm. On adult Day 2 (AD 2), intestinal VVs (~200 nm in diameter) are smaller than gonadal yolk organelles (YOs, ~500 nm in diameter). VVs, PYPs, and YOs share a uniform medium electron density by conventional EM. The morphological profiles documented in this study serve as a reference for future studies of VITs/yolk proteins.

Keywords: vitellogenin; yolk; immuno-EM; exocytosis; *Caenorhabditis elegans*

Introduction

Large lipid transfer proteins (LLTPs) play an essential role in lipid circulatory transportation, and they are found in nearly all metazoans [1, 2]. Vitellogenin (VIT)-like family, apolipoprotein B-like family, and microsomal triglyceride transfer protein (MTP) family are three major families of LLTPs [1, 2]. All LLTPs likely originate from an ancient VIT [1]. VITs, MTPs, and apolipoprotein B all have a conserved lipid-binding domain named vitellogenin_N, which forms a cavity into which lipid molecules are loaded [3].

VITs are precursors of yolk proteins. They are synthesized by oviparous animals in certain somatic cells outside the gonad, e.g., the fat body of insects, the intestine of sea urchins, and the liver of fish, birds, or amphibians. After being post-translationally modified in the endoplasmic reticulum (ER) and the Golgi apparatus, VITs are secreted as lipoprotein complexes, transported to and deposited into oocytes as nutrients for the development of embryos [4, 5]. Many studies have shown that receptor-mediated endocytosis mediates the uptake of VITs into oocytes, but how VITs are secreted is studied less [5–7].

The *Caenorhabditis elegans* animal model has six VIT proteins, VIT-1 to VIT-6. All the six VIT proteins have the same modular design, consisting of a signal peptide at the N-terminus, followed by a vitellogenin_N domain, a DUF1943 domain of unknown function, and a cysteine-rich von Willebrand factor type D (VWD) domain, which is illustrated in Fig. 1a using VIT-2 as an example. Analyzing the sequences of the six *C. elegans* VITs, we found that VIT-1 and VIT-2, precursors of the yolk protein YP170B, share 93.9% sequence identity. VIT-3, VIT-4, and VIT-5 are nearly identical precursors of YP170A. It is difficult to separate the YP170A proteins from the YP170B proteins on SDS-PAGE because they are similar in size. Peptide sequencing by mass spectrometry analysis can distinguish them because there is less than 60% sequence identity between the two groups of proteins. VIT-6 is the most divergent member. It shares only ~30% sequence identity with either VIT-2 or VIT-5, and it goes through one more round of cleavage after it is processed into YP180, which leads to the formation of YP88 and YP115 (Fig. 1b) [8]. There are two yolk protein complexes, called B dimer and A complex [9]. B dimer consists of two copies of YP170B, or VIT-1/2. A complex consists of one copy of YP170A (VIT-3/4/5), YP88, and YP115 [7, 9] (Fig. 1c). Both complexes contain about 15% lipids by weight [9].

Yolk proteins are the most abundant proteins in adult *C. elegans* hermaphrodites [8, 10, 11]. VITs are synthesized in the intestine, starting at the time of L4/adult molting [12]. Expression of the *vit* genes is turned on by a homeobox transcription factor CEH-60

Received 5 April 2024; revised 22 May 2024; accepted 12 June 2024.

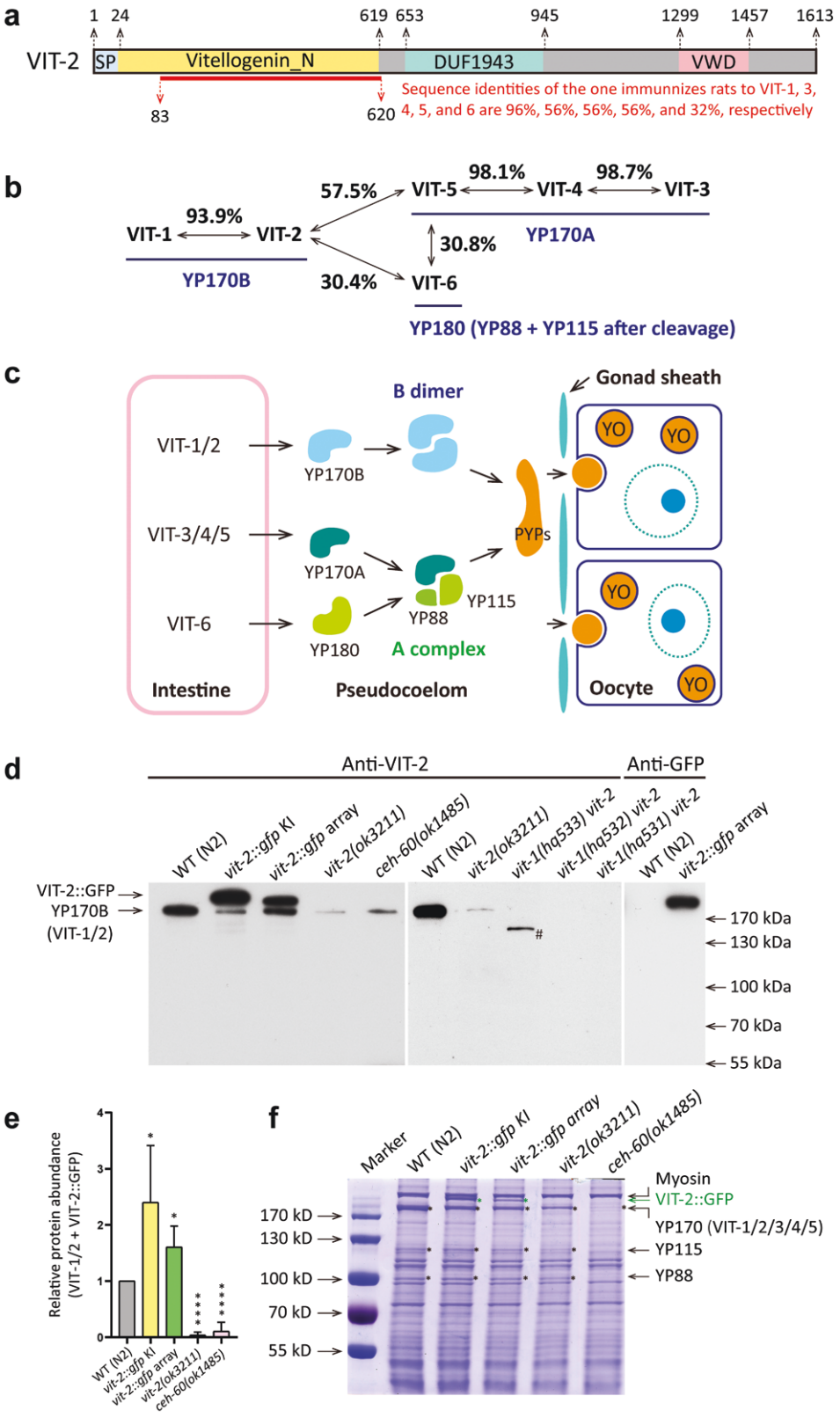

Figure 1 The VIT-2 antibody specifically recognizes YP170B, of which VIT-2 is the major isoform and VIT-1 the minor isoform. (a) Protein domains of VIT-2. SP, signal peptide; VWD, von Willebrand factor type D. The amino acid positions are indicated above the schematic diagram and the fragment (VIT-2 83–620 amino acids) used to immunize rats is indicated below with a bold line, along with the protein sequence identities between VIT-2 and other VITs within this region. (b) VITs, the corresponding yolk proteins, and the sequence identities among the full-length proteins. (c) Formation and deposition of two types of yolk protein complexes. YO, yolk organelle; PYPs, pseudocoelomic yolk patches. (d) Anti-VIT-2 and anti-GFP Western blot assay of whole-worm lysates. # indicates a mutated VIT-1 fragment expressed from *vit-1(hq533)*. (e) Quantification of anti-VIT-2 Western blot assay in (d). The intensities of YP170B and VIT-2::GFP, if present, are summed together and normalized against the WT. The bar graph displays the Mean ± STD of eight biological repeats. $^{*}P < 0.5$, $^{****}P < 0.0001$ by one-way ANOVA with Tukey's multiple comparisons test. All raw data of Western blot assay are shown in the Supplementary data—Blot Transparency. (f) Coomassie-stained SDS-PAGE of whole-worm lysate to compare the amounts of yolk proteins.

(*C. elegans* homeobox) and others [13–15]. After VITs are synthesized and their signal peptides are removed, they are secreted by the intestinal cells to the pseudocoelom, which is sometimes referred to as the body cavity. There, they are taken up by developing oocytes through receptor-mediated endocytosis (RME)-2-mediated endocytosis [6]. It is shown that oocytes take up yolk proteins directly from the body cavity through pores in the gonad sheath [16]. Yolk proteins are stored in late-stage oocytes and early embryos in membrane-bound vesicular structures called yolk organelles (YOs), also known as yolk granules, yolk spheres, or yolk platelets [16–19]. In recent years, studies have shown that continued production of yolk proteins after the end of the reproductive period causes detrimental aging phenotypes and shortens lifespan [11, 20–24].

Despite 40 years of research on *C. elegans* VITs, it is not entirely clear how VITs are secreted out of the intestine. The subcellular structures containing VIT/yolk protein are characterized insufficiently in *C. elegans*, especially those located in the intestine. For instance, a literature search found that two morphologically distinct electron microscopy (EM) structures in the intestine are both labeled as yolk granules [25, 26], and their precise membrane structures are not discernable. This has to do with a lack of systematic and high-resolution immuno-EM analysis of VIT/yolk protein [16, 18, 19, 27].

Using immuno-EM coupled with high-pressure freezing and other microscopy methods, we characterized systematically and quantitatively the VIT- or yolk protein-containing subcellular structures in *C. elegans*. More than validating previously characterized YOs and pseudocoelomic yolk patches (PYPs) with finer resolution, this study identified with precision the VIT-containing structures in the intestine, which suggested that VITs are secreted via classic exocytosis from the intestine to the pseudocoelom. We clarified that the intestinal VIT vesicles (VVs) are enclosed by a single lipid bilayer membrane, different from YOs in size, but similar to YOs and PYPs in electron density. This work lays the foundation for further studies on yolk proteins.

Results

The anti-VIT-2 antibody specifically recognizes YP170B or VIT-1/2

To document VIT- or yolk protein-containing subcellular structures by immuno-EM, we started by characterizing an anti-VIT-2 antibody. This antibody was generated by immunizing rats with a purified recombinant protein of VIT-2 (amino acids 83–620)::6 × His (Fig. 1a) [28]. Western blotting analysis indicated that the anti-VIT-2 antibody recognized a single protein band from the lysate of wild-type (WT) worms, which was markedly reduced, but not eliminated, by deletion of either *vit-2* or *ceh-60* (Fig. 1d and e) [15]. The *ceh-60* mutant has greatly reduced yolk protein levels [14], as confirmed by SDS-PAGE (Fig. 1f). Apart from VIT-2, this antibody may recognize other VITs, VIT-1/3/4/5/YP180. We highly suspect that the remaining signal on the Western blot likely comes from VIT-1, since VIT-1 and VIT-2 share 93.3% sequence identity across the full length and 96.1% identity across the fragment that was used to generate the antibody (Fig. 1a and b). We thus constructed three *vit-1 vit-2* double knock-out strains, and the remaining signal disappeared in all of them (Fig. 1d). Therefore, this polyclonal antibody recognizes both VIT-2 and VIT-1.

VIT-2 is found in all VIT- or yolk protein-containing structures in *C. elegans*

We then asked whether this anti-VIT-2 antibody can label all VIT/yolk protein-containing structures in *C. elegans*. Both VIT-1 and VIT-2 can form the B-dimer complex, while VIT-3/4/5 and VIT-6 form the A complex (Fig. 1c) [7, 9]. However, it is unclear whether these yolk protein complexes amalgamate together or whether they are packed separately, for example, VIT-1-only or A complex-only YOs. Knowing the answer to this question will facilitate the interpretation of the immuno-EM data and determine whether all the six VITs share the same pathway of transportation from the intestine to oocytes.

Using the CRISPR genome editing method [29], we engineered three dual fluorescence reporter strains: *vit-1::mCherry vit-2::gfp*, *vit-2::gfp vit-3::mCherry*, and *vit-2::gfp vit-6::mCherry*. To differentiate the signals of the fluorescent fusion proteins from the auto-fluorescence emitted by gut granules (GGs), a type of lysosome-related organelles that are found abundantly in the intestine [30–33], we acquired epifluorescent images in green, red, and blue channels (Fig. 2; Supplementary Figs. S1 and S2). The blue fluorescence signals were used to subtract autofluorescent objects. After subtraction, we quantified the colocalization rate of the GFP signal and the mCherry signal in each of the rectangular regions of interest (ROI) distributed in the imaged intestine, pseudocoelom, oocytes, and embryos (10–70 images of 10–31 worms for each category, 3 ROIs per images, 60–200 μm^2 per ROI). Other details about the quantification analysis can be found in Supplementary Fig. S1d–i and the "Materials and methods" section. On average, ≥ 93% of the VIT-2::GFP signals colocalized with the mCherry signals of VIT-1, -3, and -6 (Fig. 2; Supplementary Fig. S1a–c). These results suggest that A complex and B dimer colocalize, and the B-dimer subspecies (VIT-1 homodimer, VIT-2 homodimer, and VIT-1/VIT-2 heterodimer, if there are) also colocalize. Therefore, the transportation route to be mapped using the anti-VIT-1/2 antibody should be an inclusive one for all VITs/yolk proteins.

VVs in the intestine are smaller than gonadal YOs

Next, we performed immuno-EM analysis. In adult Day 2 (AD 2) WT hermaphrodites, the anti-VIT-1/2 antibody targeted gold particles to YOs in embryos and oocytes (Fig. 3a–f), in which YOs have been well characterized [16, 18]. Consistent with previous reports, the observed gonadal YOs were vesicular structures of ~0.5 μm in diameter (Fig. 3b, f, and i). The lipid bilayer membrane of YOs was preserved thanks to the high-pressure freezing method (Fig. 3b).

In addition to YOs in the gonad, anti-VIT-1/2 immuno-gold particles labeled similar but much smaller vesicular structures inside the intestine (Fig. 3g and h). The average diameter of these VIT-containing structures was only 0.2 μm (Fig. 3i), and we named them VVs because two mature yolk proteins YP115 and YP88 do not form until VIT-6 is secreted out of the intestine [8]. VVs were also identified by anti-GFP immuno-EM in the *vit-2::gfp* knock-in (KI) worms and their lipid bilayer membrane was confirmed (Fig. 3j–m).

Classic exocytosis mediates VIT secretion from the intestine to the pseudocoelom

In intestinal cells where VIT proteins are synthesized, we observed anti-VIT-1/2 gold particles on the rough ER and the Golgi apparatus (Fig. 4a–d). This is consistent with VITs as secreted proteins, each containing a signal peptide for docking onto the ER [34]. Quantitation of the micrographs showed that the density of the immuno-gold particles in areas of stacked ER was significantly higher than those that did not contain VITs (e.g., mitochondria and lipid droplets) (Fig. 4e), which is consistent with the notion that VITs are synthesized in the ER of

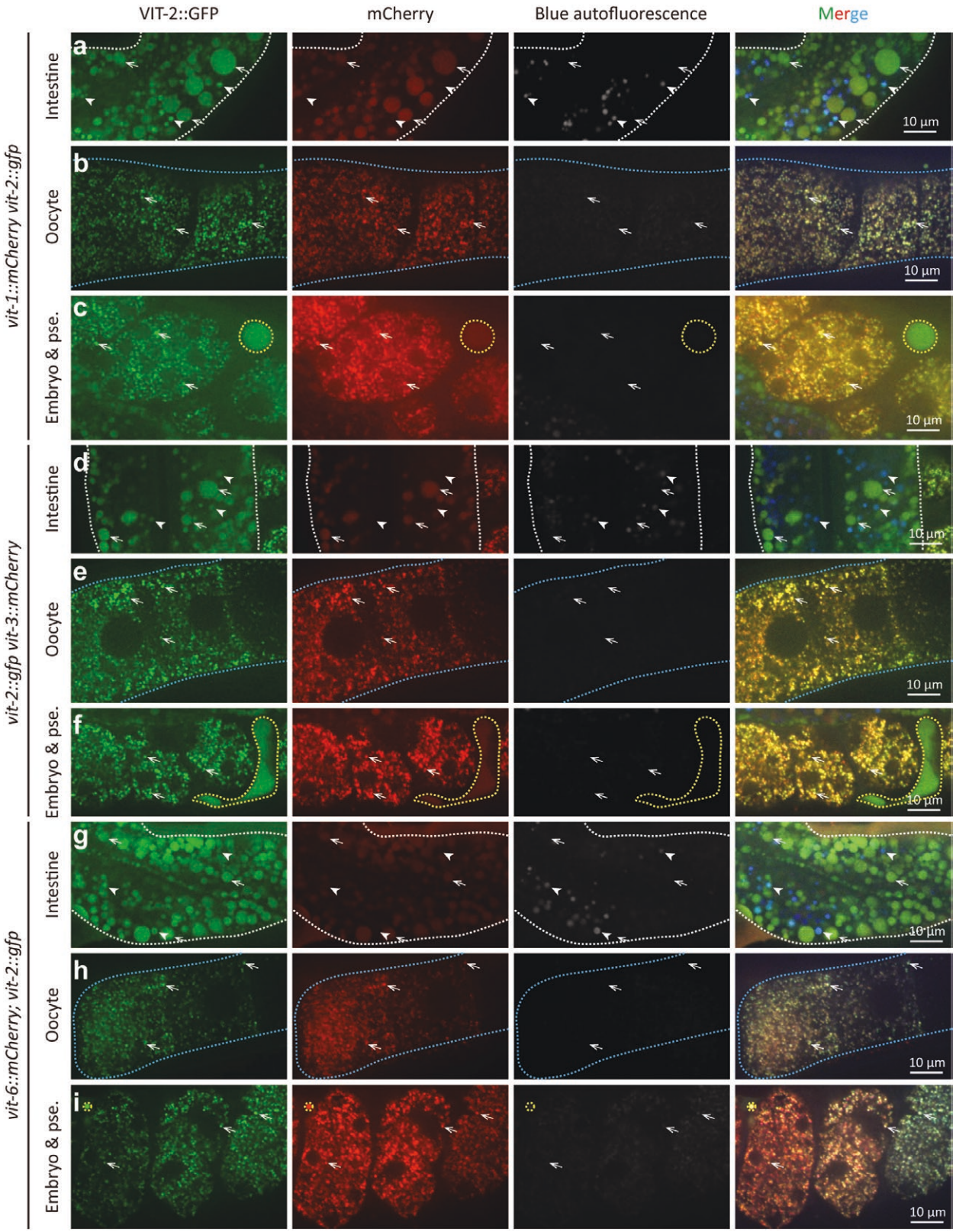

Figure 2 Colocalization among *C. elegans* VITs. Fluorescent images of *vit-1::mCherry vit-2::gfp* (a–c), *vit-2::gfp vit-3::mCherry* (d–f), and *vit-2::gfp vit-6::mCherry* (g–i) KI worms at AD 2. (a, d, and g) White dots outline the intestine, arrows point to VVs, and arrowheads indicate GGs, which emit strong green and blue auto-fluorescence. (b, c, e, f, h, and i) Arrows point to YOs in oocytes and embryos. Blue and yellow dots outline the oviduct and a PYP, respectively.

intestinal cells [35, 36]. The ER exit site is where secretory proteins are packaged into transport vesicles coated with protein complex II (COPII), which then bud off and move to the Golgi [37]. One previous study showed that knocking down *sft-4* (the worm ortholog of surfeit locus gene *Surf-4*), *sec-23*, and *sar-1* (secretion-associated RAS-related protein 1)—three genes required for ER

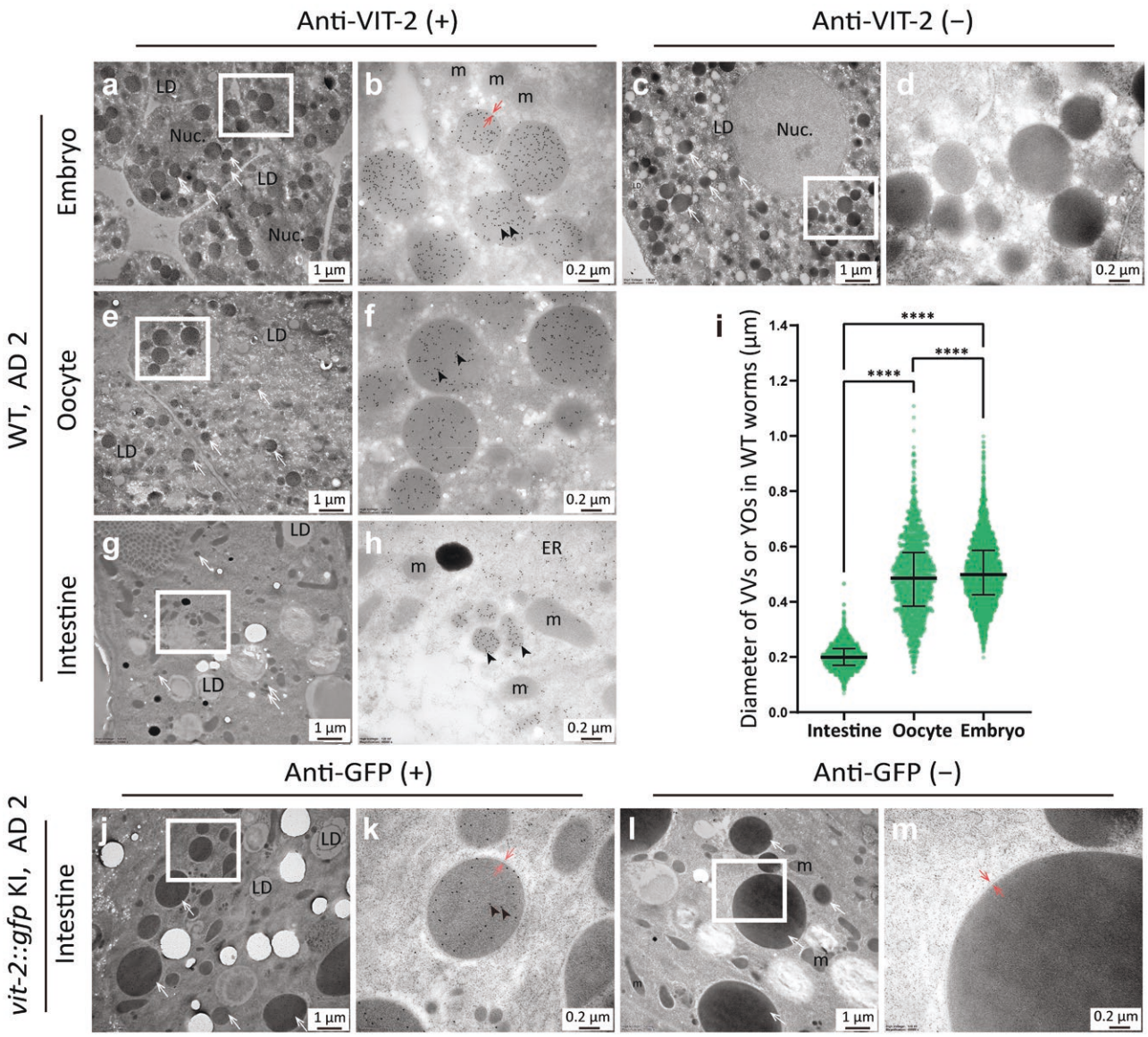

Figure 3 Morphology of intestinal VVs and gonadal YOs in young adult *C. elegans*. (a–i) Immuno-EM of WT worms on AD 2. (a and b) Micrographs showing anti-VIT-2 immuno-gold labeling of YOs in unlaid embryos in the uterus. (c and d) Negative control of (a) and (b), in which samples were processed without incubation with the anti-VIT-2 antibody. (e–h) Micrographs showing YOs in oocytes (e and f) and VVs in the intestine (g and h) labeled by anti-VIT-2 gold particles. (i) Size analysis of VVs in the intestine, YOs in oocytes, and YOs in unlaid embryos from 217, 58, and 88 micrographs, respectively. For each, the median diameter is indicated along with the interquartile range. $^{****}P < 0.0001$, one-way ANOVA with Tukey's multiple comparisons test. (j–m) AD 2 worms expressing VIT-2::GFP from a KI allele. Micrographs showing Anti-GFP antibody targeted immuno-gold particles to intestinal VVs (j and k). There was no gold particle labeling in the anti-GFP (–) negative control (l and m). Black arrowheads point to the 10-nm (b, f, and h) or 12-nm (k) gold particles and white arrows point to gonadal YOs (a, c, and e) or intestinal VVs (g, j, and l). Paired red arrows indicate the lipid bilayer membrane. The regions framed by white rectangles are magnified and shown on the right (b, d, f, h, k, and m showing the boxed regions in a, c, e, g, j, and l, respectively). Nuc.: nucleus; LD: lipid droplet; m: mitochondrion; ER: endoplasmic reticulum.

exit site assembly—causes VIT retention in the intestinal ER lumen via fluorescent microscopy [36].

In other species, including fish, it is reported that VITs are secreted through classic exocytosis [38, 39]. How VITs in *C. elegans* are secreted from the intestine to the pseudocoelom is a topic hardly discussed in the literature. A previous genome-wide RNAi screen [35] identified candidate genes that affected VIT secretion, but these candidates were not validated or studied further. In immuno-EM images, anti-VIT immuno-gold labeled the ER, the Golgi apparatus, and the VVs, in addition to gonadal YOs (Fig. 4). The gold particle labeling was also detected on yolk pit structures along the basal membrane of intestinal cells (Fig. 5a and b). These yolk pit structures could represent a stage right after vesicle-plasma membrane fusion when the content of the vesicle is being emptied out or the beginning of endocytosis. Light microscopy of worms expressing VIT-2::GFP seemed to support the exocytosis interpretation better (Fig. 5c–e). Pseudocoelomic yolk was not bound by a lipid membrane and was widespread in the pseudocoelom of older worms (AD 6) (Fig. 5f), which is consistent with an earlier finding [27]. Taken together, the evidence above points to a classic secretory pathway from the ER to the Golgi, then to exocytic vesicles, and lastly to the extracellular space after the vesicles fuse with the plasma membrane (Fig. 5g) [40].

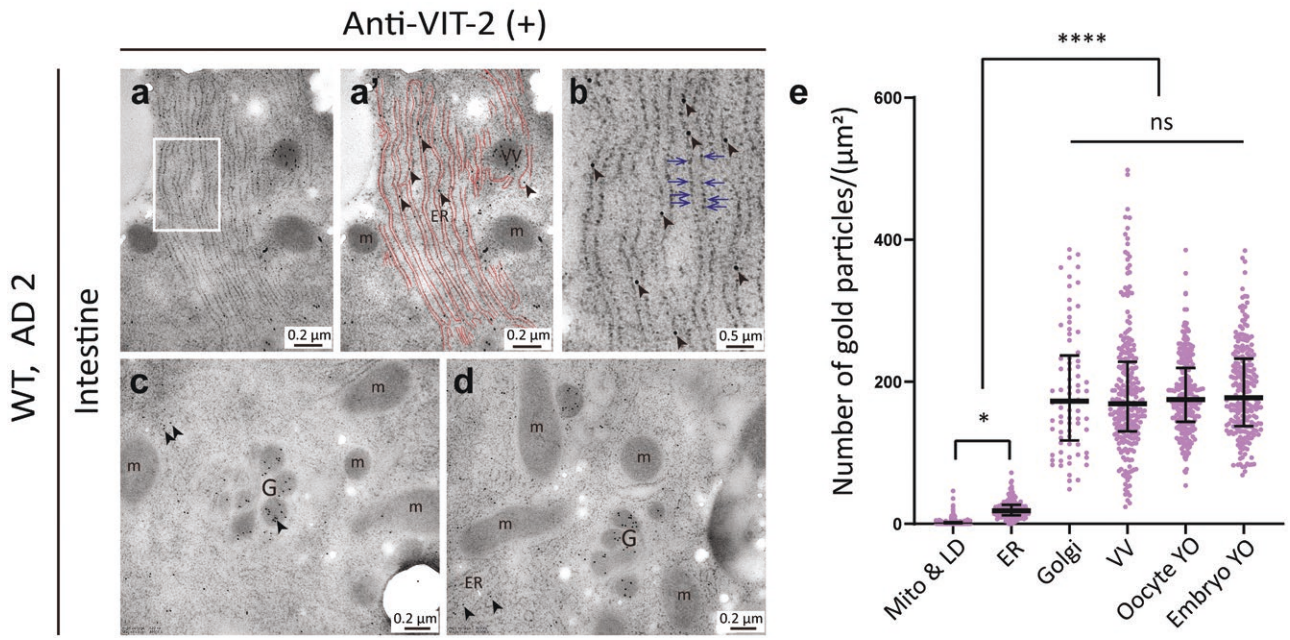

Figure 4 Anti-VIT-2 immuno-gold labeling of the ER and the Golgi apparatus of intestinal cells. (a and b) Micrographs showing gold particles attached to the ER. (a) An area of stacked ER labeled by gold particles. (a') The membrane of ER in (a) is traced by red lines. (b) Magnified view of the boxed region in (a). (c and d) Micrographs of the Golgi labeled by gold particles. ER: endoplasmic reticulum; m: mitochondrion; VV: vitellogenin vesicle; G: the Golgi apparatus. Black arrowheads point to gold particles, blue arrows point to the ribosomal particles attached to the ER. (e) The density of gold particles on different subcellular structures. Measurements were based on 39, 39, 25, 44, 26, and 23 micrographs for mitochondrion and lipid droplet (mito & LD), ER, Golgi, VV, oocyte YO, and embryo YO, respectively. The median value and the interquartile range are indicated. $^{*}P < 0.05$, $^{****}P < 0.0001$, ns, not significant by one-way ANOVA with Tukey's multiple comparisons test.

The size of VV is correlated with the total amount of VIT proteins

After we analyzed VIT-containing structures in WT *C. elegans*, we asked how these structures might be affected when VIT proteins were deficient or overly abundant. As verified by SDS-PAGE (Fig. 1f), the yolk protein levels were reduced in the *vit-2* mutant and more so in the *ceh-60* mutant [14, 15] (Fig. 6a–l). The size and the number of intestinal VVs were decreased in both mutants (Fig. 6m and n, WT > *vit-2* > *ceh-60*), whereas gonadal YOs were affected less (Fig. 6o). There was no difference in YO sizes between WT and *vit-2(ok3211)* worms, while YOs of the *ceh-60(ok1485)* worms were smaller than that of WT YOs by about one-third in diameter (Fig. 6o).

The *C. elegans* strain harboring a *vit-2::gfp* array overexpressed VIT-2::GFP, as did the *vit-2::gfp* KI strain for unknown reasons (Fig. 1d and e). In both strains, intestinal VVs enlarged 3–9 times in diameter compared to the WT (Fig. 7a–h; Supplementary Fig. S3). Consequently, a larger intestinal area (9%–13%) was occupied by VVs in these strains compared to that of WT (only 1% of which was occupied) (Fig. 7i). However, an overabundance of VIT-2::GFP did not increase the size of gonadal YOs. Rather, gonadal YOs were slightly smaller in worms carrying either the *vit-2::gfp* KI allele or the *vit-2::gfp* array (Fig. 7j).

Taken together, the data above suggest that the size of intestinal VVs but not gonadal YOs is correlated positively with the total amount of VIT proteins in the worm. The size of gonadal YOs can be affected by but is not correlated with the total VIT protein level.

Morphology of VIT- or yolk protein-containing structures in conventional EM

Lastly, to help researchers better identify VVs and YOs using conventional electron micrographs, we followed a previously described approach [41] and processed two consecutive EM sections differently, and then registered and compared the structures on the neighboring sections. Fig. 8a presents an immuno-EM image of the intestine of a WT worm on AD 6, in which a VV was labeled by gold particles. Fig. 8b shows the adjacent section, which was not incubated with the antibody; rather, it was stained and collected as if it were a conventional EM section. In other words, Fig. 8b represents a hybrid sample preparation method, in which the samples were processed in the earlier steps for immuno-EM and the later steps for conventional EM. This allowed us to unambiguously identify which vesicular structures in the intestine were VVs and which ones were not (Fig. 8c). The typical morphology of AD 2 intestinal VVs, AD 6 gonadal YOs, and AD 6 PYPs were displayed in Fig. 8d–i as a reference. Note that intestinal VVs were larger in older adults (compare panels a–c with panels d–f of Fig. 8), as described elsewhere in greater detail [42]. The morphology of PYPs examined by conventional EM (Fig. 8c and i) was the same as that examined by immuno-EM (Fig. 5f), and was consistent with what has been reported before [27].

Discussion

Yolk protein complexes are intermingled

Colocalization of VIT-2::GFP and mCherry-tagged VIT-1, VIT-3, and VIT-6 suggests that B dimer (VIT-1/2) and A complex (VIT-3/4/5 and VIT-6) are packed as a mixture into VVs and YOs. The existence of a VIT-1/VIT-2 heterodimer is supported by a previously reported unbiased chemical cross-linking experiment using *C. elegans* protein samples (Supplementary Table S1) [43]. From this dataset, we found five cross-links between VIT-1 and VIT-2 after applying a stringent filter (#spectra ≥ 3, best E-val < 1.0×10^{-7}, FDR < 5%). For A complex, we found five cross-links between VIT-3/4/5 and VIT-6 and one cross-link between

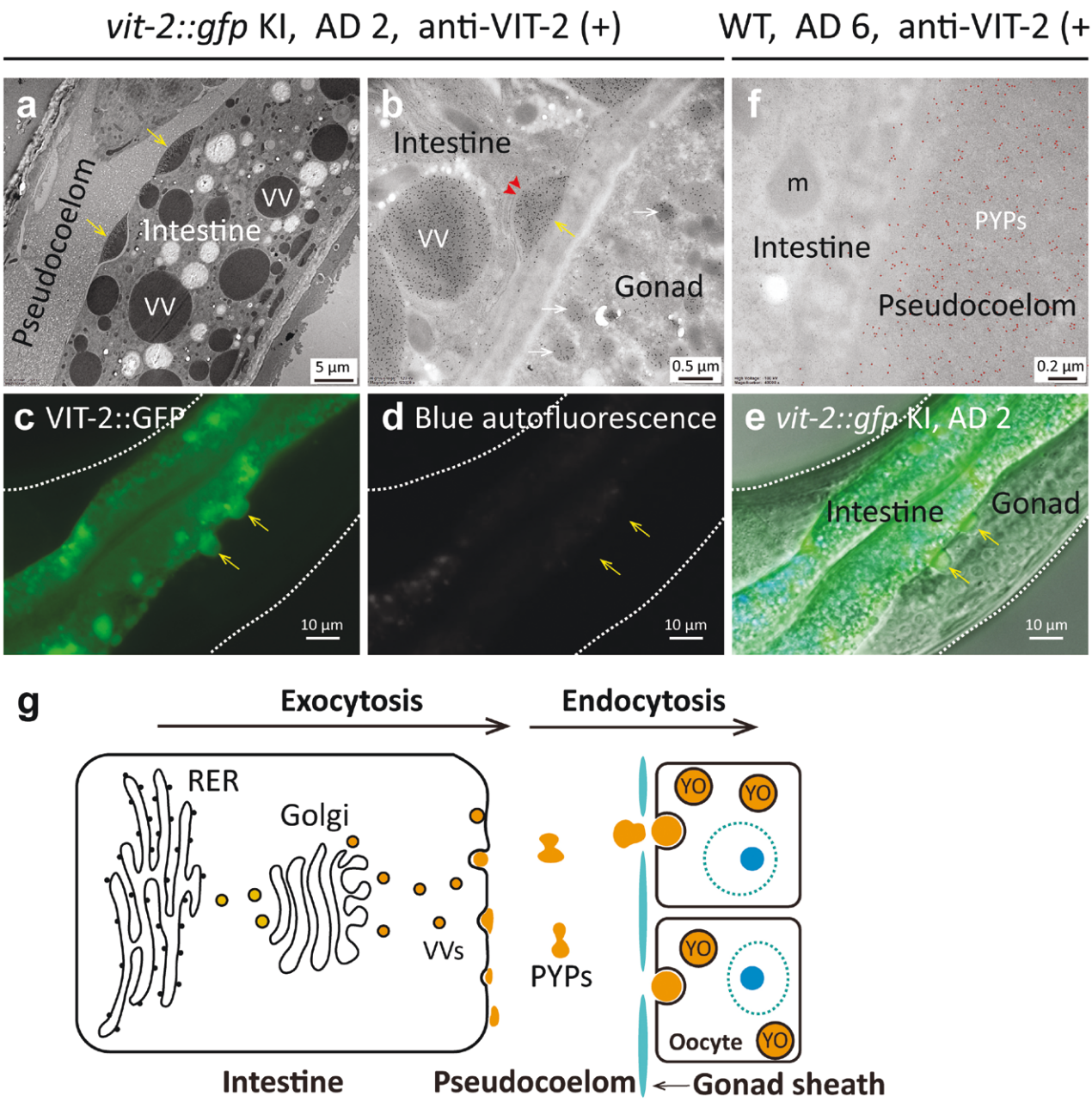

Figure 5 More evidence for exocytosis mediating VIT secretion from the intestine to the pseudocoelom. (a, b, and f) Anti-VIT-2 immuno-EM of the *vit-2::gfp* KI worms on AD 2 (a and b) or the WT worms on AD 6 (f). Yellow arrows point to patches of yolk that appear to be at the final stage of exocytosis from the intestine to the pseudocoelom (a–e). Red arrowheads point to the basal membrane of the intestine, and white arrows indicate YOs in the gonad (b). Red dots mark the 10-nm gold particles seen on a patch of yolk in the pseudocoelom (f). (c–e) Fluorescence imaging captured VIT-2::GFP positive vesicles being released to the pseudocoelom. (g) A model illustrating that VITs are secreted to the pseudocoelom through exocytosis. RER: rough ER; PYPs: pseudocoelomic yolk patches.

VIT-3/4 and VIT-6. There was also one cross-link between B dimer and A complex (VIT-2(K972)–VIT-3/4/5(K1201)), suggesting that B dimer and A complex may form a higher-level complex.

mCherry-tagged VIT-1/3/6 appeared brighter in developing embryos than in the intestine, and the opposite can be said about VIT-2::GFP (see Supplementary Fig. S4a–c as an example). As YOs are latent lysosomes [44], the intensity difference of mCherry and GFP in developing embryos likely results from the acidification of YOs, which activates the lysosomal hydrolases to break down yolk proteins to support embryonic development. Under the acidic pH of the lysosome, GFP loses but mCherry retains fluorescence [45]. The intensity difference of mCherry and GFP in the intestine or oocytes may be related to the different expression levels of VIT-2 and VIT-1/3/6, at least in part. Mass spectrometry data suggest that VIT-2 and VIT-6 are expressed at higher levels than VIT-1 and VIT-3 in WT worms, as the integrated whole-organism protein abundance values for VIT-1, -2, -3, and -6 are 1345, 2554, 1196, 3091 parts per million, respectively (pax-db.org, *C. elegans*-Whole organism, SC (Peptideatlas, Jun, 2016)). Other possible reasons include the difference in maturation time between mCherry and GFP, and a greater tendency to aggregate for red fluorescent proteins as discussed before [46–50].

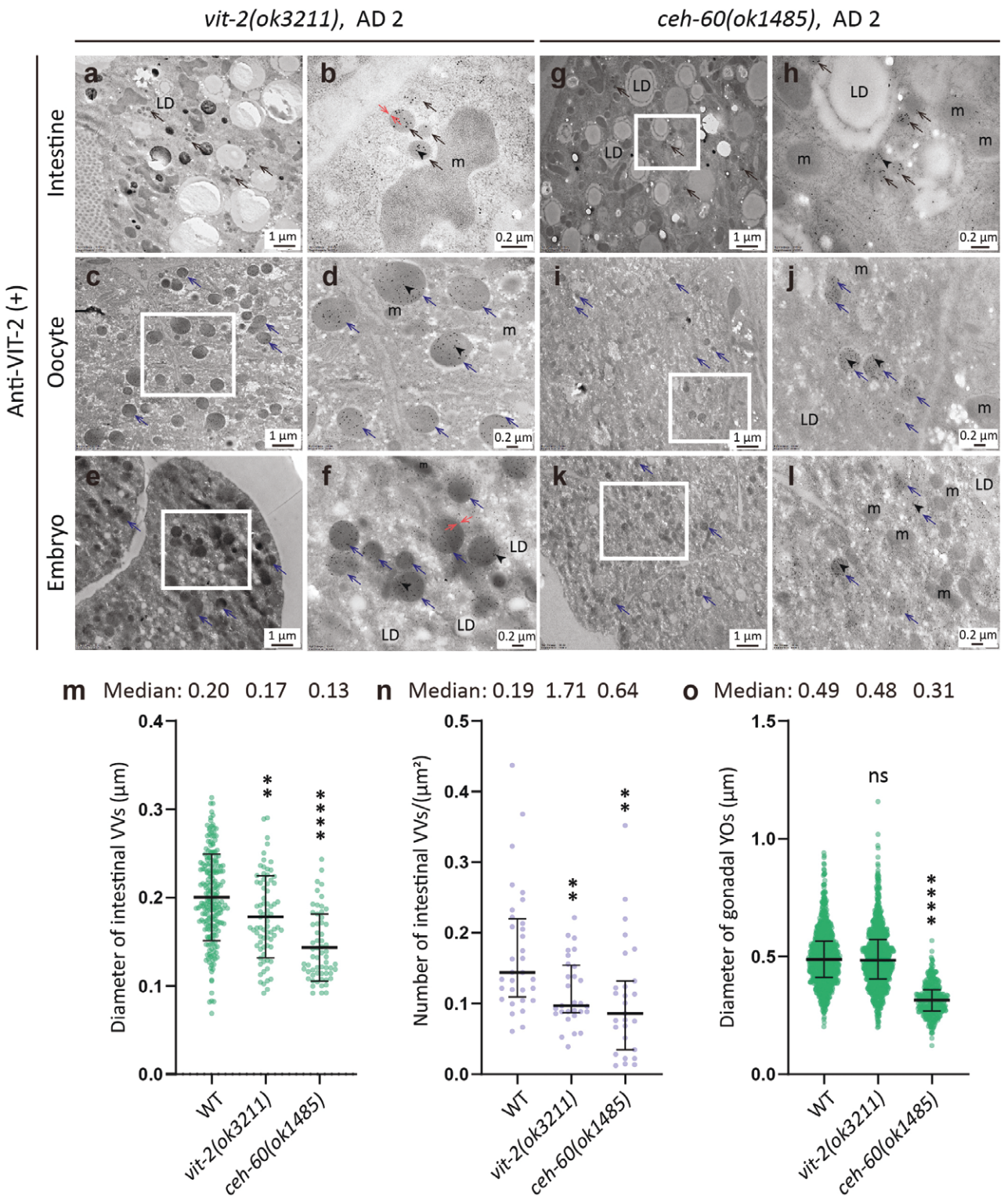

Figure 6 VVs and YOs in VIT-deficient mutants. (a–l) Anti-VIT-2 immuno-EM of the *vit-2(ok3211)* mutant (a–f) or the *ceh-60(ok1485)* mutant (g–l) on AD 2. The boxed regions are magnified and shown on the right. Black arrowheads point to gold particles, black arrows point to intestinal VVs, and blue arrows point to YOs. The lipid bilayer membrane enclosing VVs or YOs is indicated by a pair of red arrows. LD: lipid droplet; m: mitochondrion. (m–o) Quantitative comparison of VVs and YOs between WT and VIT-deficient mutant worms. For WT (N2), *vit-2(ok3211)*, and *ceh-60(ok1485)* worms, 17, 22, and 17 micrographs were quantified for determining the diameter of intestinal VVs (m), 32, 29, and 27 micrographs for the density of intestinal VVs (n), 21, 26, and 25 micrographs for the diameter of gonadal YOs (o), respectively. $^{**}P < 0.01$, $^{****}P < 0.0001$, ns, not significant, all compared to WT by one-way ANOVA with Tukey's multiple comparisons test.

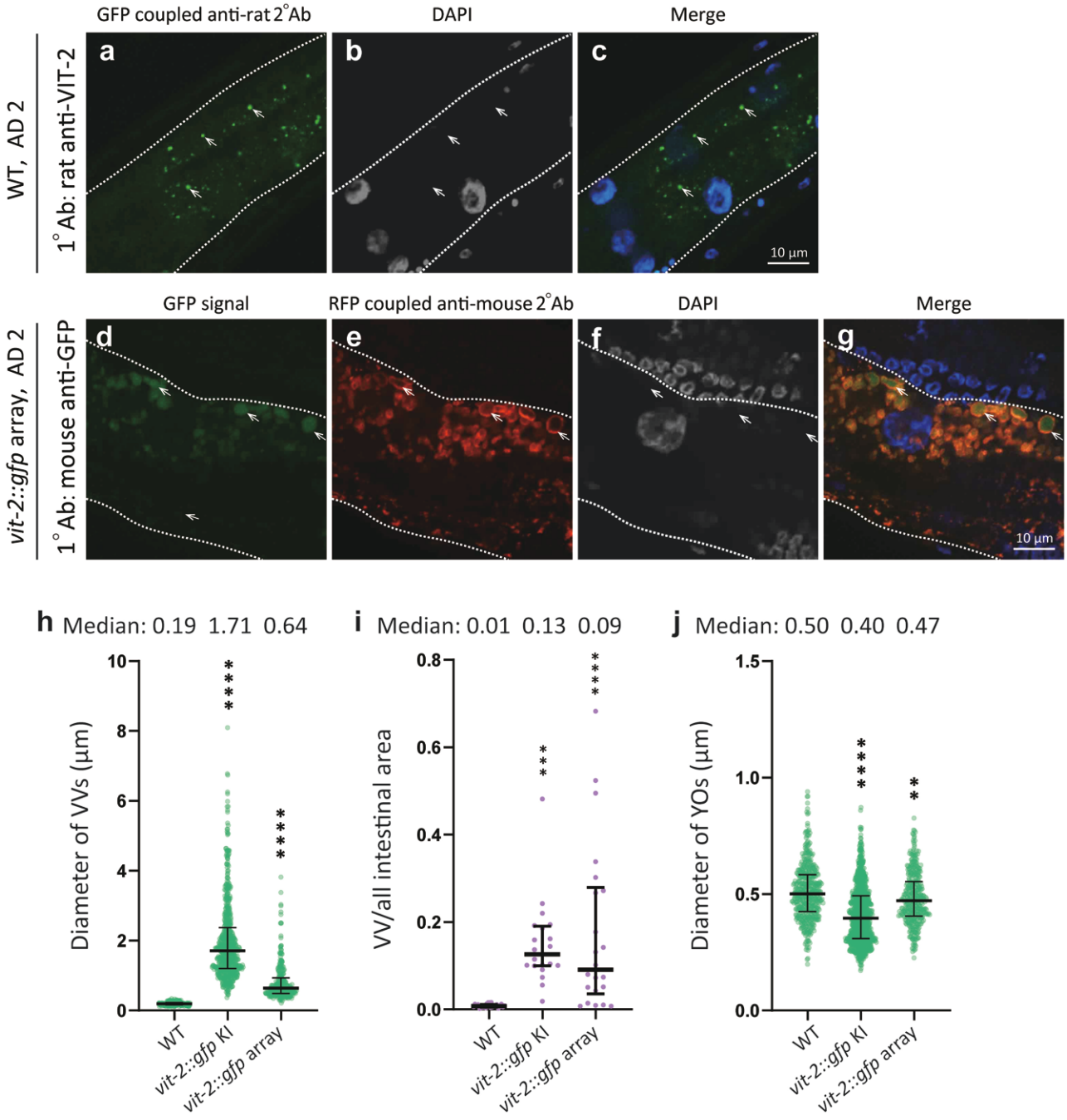

Figure 7 VVs and YOs in worms overexpressing VIT-2::GFP. (a–c) Anti-VIT-2 immuno-fluorescence (IF) staining of WT *C. elegans* on AD 2. (d–g) Anti-GFP IF staining of the VIT-2::GFP overexpressor on AD 2. The GFP tag retained its green fluorescence after IF staining. White dots outline the intestine. (h–j) Quantification of the diameter of intestinal VVs (h), the ratio of VV area to total intestinal area (i), and the diameter of gonadal YOs (j) in WT and two VIT-2::GFP overexpression strains. In the *vit-2::gfp* KI strain, the GFP coding sequence was knocked into the *vit-2* gene locus, which would in theory result in VIT-2::GFP being expressed at or near the endogenous VIT-2 level. However, VIT-2::GFP was somehow expressed at a higher level as shown in Fig. 1d and e. For WT (N2), *vit-2::gfp* KI, and *vit-2::gfp* array strains, 25, 21, and 22 micrographs were quantified for VVs (h), 25, 20, and 22 micrographs were quantified for the ratio of VV area (i), 11, 14, and 11 micrographs were quantified for YOs (j), respectively. The median and interquartile range are indicated. $^{**}P < 0.01$, $^{****}P < 0.0001$, all compared to WT by one-way ANOVA with Tukey's multiple comparisons test.

Maturation of yolk protein complexes along the exocytic pathway

The immuno-EM images in this study revealed the presence of VITs in the intestinal cells along the exocytic route, from the rough ER to the Golgi and then secretory vesicles.

It is predicted that all the six VITs likely have a signal peptide and should direct their synthesis on the rough ER [34]. In line with this prediction are several lines of experimental evidence. Firstly, VIT-2::GFP accumulates in the ER when the ER exit site is compromised [36]. Secondly, yolk proteins are strong concanavalin A (Con A) binders [10], which suggests that yolk proteins likely have high-mannose N-glycans, which are attached to proteins in the ER [51]. Thirdly, yolk proteins have intra- and inter-chain disulfide bonds [9], which are normally formed in the ER [52]. Lastly, yolk

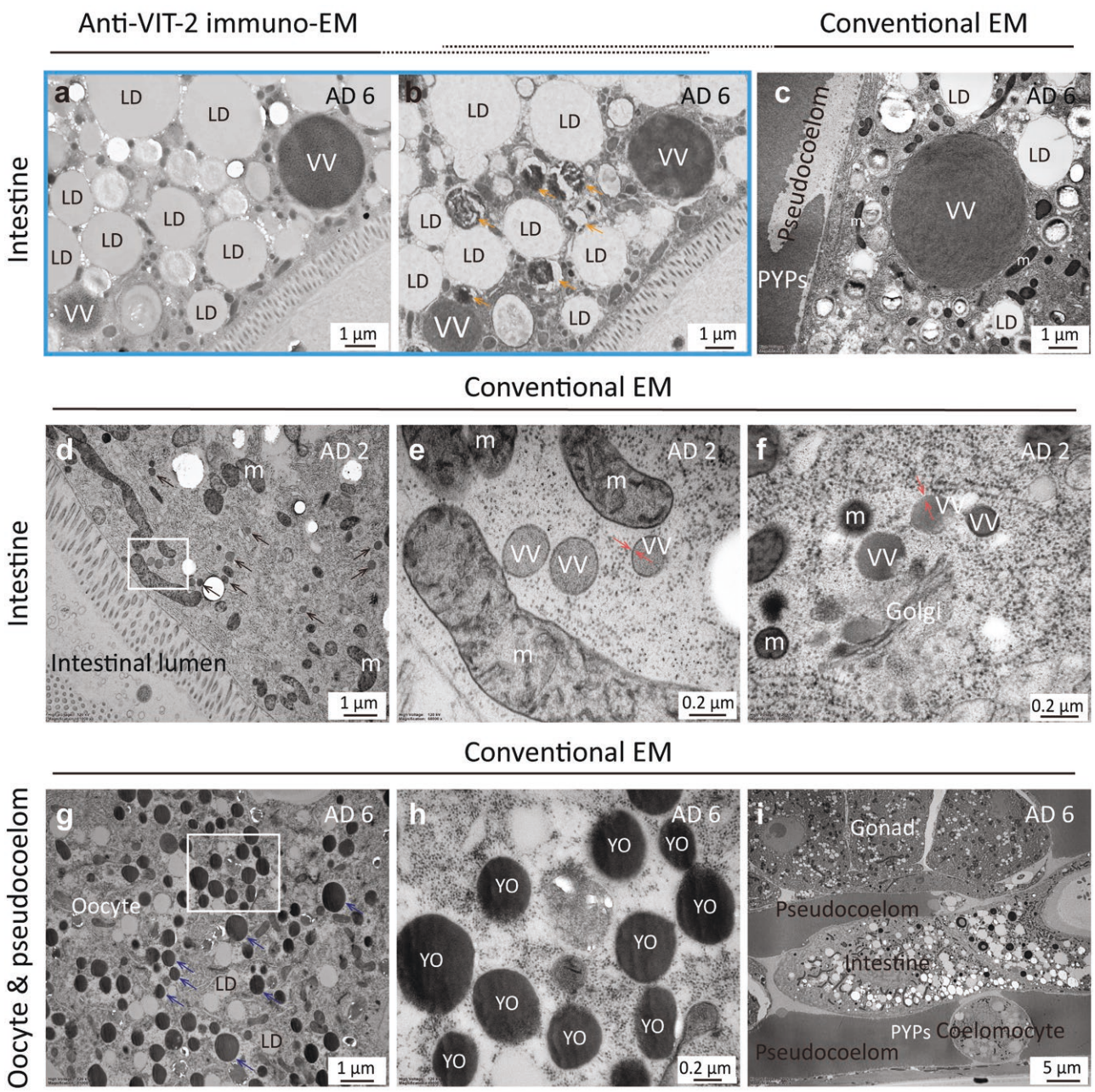

Figure 8 Morphology of intestinal VVs, gonadal YOs, and PYPs under conventional EM. (a–c) Micrographs of intestinal VVs of WT worms on AD 6. (a) Anti-VIT-2 immuno-EM. (b) An adjacent section of the one shown in (a), not incubated with antibodies and colloidal gold particles, but stained with lead citrate and uranyl acetate as in conventional EM, collected on carbon-treated tape, and imaged by scanning EM. (c) Conventional EM, imaged by TEM. (d–f) Conventional TEM of intestinal VVs of WT worms on AD 2. (g–i) Conventional TEM of WT worms on AD 6, highlighting YOs in oocytes (g and h) and PYPs (i). The boxed regions in (d) and (g) are shown at higher magnification in (e) and (h), respectively. The micrographs are marked in the same way as in Fig. 6, except for the orange arrows that depict the micrometer-sized dark inclusion bodies in Fig. 8b.

protein complexes contain 15% lipids by weight [9], including 8.5% phospholipids, ~3% triacylglycerol, and ~3% other lipids. Lipidation of *C. elegans* VITs has not been studied. Lipidation of human apolipoprotein B-100 (ApoB-100) occurs in the lumen of rough ER, associated with MTP [53]. Both ApoB-100 and MTP are homologs of *C. elegans* VIT-1 to VIT-6 [1].

VITs of non-mammalian vertebrates are heavily phosphorylated, which could be a way of delivering phosphate to oocytes. Phosphorylation is concentrated in a small region called phosvitin, which is not found in *C. elegans* VITs. We looked up a recently published phosphoproteomics dataset and found that each of the six *C. elegans* VITs is phosphorylated at multiple sites (Supplementary Table S2) [54]. For VIT-1/2/3/4/5, phosphorylation is concentrated near the C-terminus. The phosphorylation sites (phosphosites) of VIT-6 are concentrated in the middle region and near the C-terminus.

To sum up, *C. elegans* VITs are probably large secreted lipo-glyco-phosphoproteins, like their vertebrate counterparts.

Presence of YOs in early-stage oocytes, albeit fewer than in late-stage oocytes

C. elegans hermaphrodites on AD 2 have 8–10 oocytes in each proximal gonad and they are numbered -1, -2, -3, and so on from the one that is most proximal to the spermatheca. A recent review

stated that yolk in *C. elegans* is loaded into the three most proximal oocytes [7], but a close examination of the imaging data [6, 7] found that VIT-2::GFP is present in -4, -5, and even earlier-stage oocytes, albeit at an increasingly lower level. This is consistent with what we saw by immuno-EM and confocal fluorescent microscopy (Supplementary Fig. S4).

What causes the unevenly distributed YOs in oocytes at different stages? Adult hermaphrodites have five pairs of sheath cells covering the germ cells and oocytes at each gonad arm. Pairs 3–5 sheath cells are fenestrated, and there are pores, called sheath pores, localized on sheath cells, allowing pseudocoelomic yolk to go through to reach oocytes. The three pairs of fenestrated sheath cells wrap around –1 to –6 oocytes [16, 55]. Theoretically, –1 to –6 oocytes can take up yolk directly from the pseudocoelom, but –1 oocyte contains more YOs than –2 oocyte, –2 more than –3, and so on. It is one possible explanation for the formation of this YO gradient that mature oocytes have more time to accumulate yolk. Another explanation is provided by a study on RME-2, the yolk protein receptor. Although oocytes start to express RME-2 from an early stage, several most proximal ones have more RME-2 extracellular domain—which binds to yolk proteins—exposed on the cell surface [6].

Are yolk proteins dispensable for embryogenesis?

In *ceh-60* and *vrp-1* (vitellogenin-regulating *Caenorhabditis*-specific protein) mutant worms, the amount of yolk proteins is much reduced, yet the brood size is normal and embryo development seems unaffected [13, 15, 56]. RNAi of *vit* genes has no effect on fertility, either [11]. Consequently, the notion that yolk proteins are required for *C. elegans* embryogenesis is challenged [7, 15]. Here, immuno-EM readily detected VVs and YOs in the *ceh-60* mutant, albeit of a smaller size (Fig. 6). It follows that the *ceh-60* oocytes likely have enough residual yolk proteins to support embryogenesis. As none of the existing mutations or RNAi treatments completely abolish yolk proteins, there is not enough evidence to conclude that *C. elegans* yolk proteins are dispensable for embryogenesis.

Size control of VVs and YOs

One interesting observation from this study is that intestinal VVs and gonadal YOs seem to have different size control mechanisms. The size of VVs is sensitive to VIT production, changing from 0.13 μm (65% of WT) to 1.71 μm (900% of WT) in diameter, from yolk protein deficient to overproduction strains (Figs. 6 and 7). For WT worms, as yolk proteins accumulate with age, VVs also enlarge, from 200 nm in diameter at AD 2 to 3–4 μm at AD 6 and AD 9 [42].

In contrast, the size of YOs changes little (0.31–0.48 μm in diameter), and overproduction of yolk proteins does not make bigger YOs (Figs. 6 and 7). Accumulation of yolk proteins in aged worms is not accompanied with bigger YOs, either [42]. The sheath pores or fenestrae on sheath cells are typically 100–300 nm in diameter [16]. When PYPs go through the sheath pores and into oocytes, the size of resulting YOs may be defined by the pores. Alternatively, the endocytosis capacity of oocytes may limit the size of YOs.

VVs are not GGs defined by light microscopy, nor the dark inclusion bodies defined by EM

VVs may be more than secretory vesicles, for example, some should be transport vesicles. Further characterization of VVs will clarify this issue. Intestinal cells are filled with vesicles of different types, one of which is autofluorescent GGs. GGs contain glycosylated anthranilic acid, which emits intense blue fluorescence under UV light [30–33]. A subset of GGs also contains birefringent materials [33]. Here we show that VVs (i.e., intestinal yolk granules) contain neither birefringent materials (Supplementary Fig. S2) nor blue fluorescent materials (Fig. 2; Supplementary Fig. S2). In other words, VVs and GGs are distinct from each other.

Prior to this study, VVs were thought to be similar to the well-characterized YOs in oocytes and embryos of mature adults, e.g., micron level in diameter and high electron density in EM [26, 57]. This notion has led to questionable identification of VVs. In two earlier conventional EM studies, the vesicles labeled as "intestinal yolk granules" were almost certainly mis-identified. In one study, the "yolk granule" label was attached to micrometer-sized dark inclusion bodies with or without a nested concentric ring of pitch-blackness in worms at the L2 or dauer larval stage [26], when *vit* genes are not yet turned on [12]. In the other study, vesicles with a nested concentric ring of pitch-blackness were labeled tentatively as "maturing yolk"? [25]. Our immuno-EM analysis found that in WT AD2 adults, VVs were of a medium electron density and ~200 nm in diameter, much smaller than gonadal YOs (~500 nm). Only in worms of high VIT levels or older age (e.g., AD 6) did we find micrometer-sized VVs (Figs. 3j–m and 8a–c).

No VITs in *C. elegans* body wall muscles

A recent study published in 2021 found, by the use of fluorescent transgene reporters, that body wall muscles of young adult *C. elegans* can synthesize VIT-2, and transport it to oocytes via VIT-2-containing exophers [58]. This finding is contradictory to that of an earlier study, which used a sensitive [^{35}S]-methionine incorporation method to label newly synthesized proteins [12]. The 1983 study found that only the dissected intestine synthesizes yolk proteins, the gonad and the body wall, which contain body wall muscle, hypodermis, and cuticle, do not [12]. Here the anti-VIT-1/2 immuno-EM analysis showed that neither the body wall muscle nor the pharyngeal muscle can be labeled by immuno-gold particles above the background (Supplementary Fig. S5m–q), which agrees with the 1983 study [12] but not the 2021 study [58].

To examine this controversy more carefully, we generated two double-labeling strains, one expressing *myo-3p*::GFP and VIT-6::mCherry and the other expressing *myo-3p*::mCherry and VIT-2::GFP. In neither strain did we detect colocalization between the red and green fluorescence signals (Supplementary Fig. S5a–l and Supplementary Fig. S5a′–l′). Given all the evidence, we are compelled to draw the same conclusion as the 1983 study, which is that *C. elegans* body wall muscles do not express VITs.

Examining the data of several tissue-specific transcriptome analyses [59–61], we found that the reads number of *vit* transcripts found in body wall muscles was not statistically different from those found in the hypodermis, pharyngeal muscles, neurons, or the negative controls. This suggests that *vit* mRNAs detected in body wall muscles are probably background noise.

Materials and methods

VIT sequence alignment

The VIT sequences were downloaded from WormBase, and then every two sequences of them were uploaded on the web tool Pairwise Sequence Alignment (via the EMBL-EBI website). The percentage identities between every two VITs (Fig. 1b) were calculated via the EMBOSS Needle method, which created an optimal global alignment of two sequences using the Needleman-Wunsch algorithm.

Worm culture and strains

Caenorhabditis elegans was fed with *Escherichia coli* OP50 on nematode growth medium (NGM) plates and cultured at 20°C. To produce synchronized cohorts of worms, 25 gravid hermaphrodites were put on a plate and allowed to lay eggs for 4 h before being taken away. Worms within 24 h after reaching sexual maturity were regarded as one day old. In this study, 13 strains were used, including wild type (N2), MQD1052 *vit-2(bIs1 [vit-2::gfp + rol-6(su1006)])* X, BCN9071 *vit-2(crg9070[vit-2::gfp])* X, MQD2798 *vit-1(hq503[vit-1::mCherry]) vit-2(crg9070[vit-2::gfp])* X, MQD2775 *vit-2(crg9070[vit-2::gfp]) vit-3(hq485[vit-3::mCherry])* X, MQD2774 *vit-6(hq486[vit-6::mCherry]) IV; vit-2(crg9070[vit-2::gfp])* X, MQD2972 *vit-6(hq486[vit-6::mCherry]) IV; qxEx3005 [myo-3p::gfp + unc-76]*, MQD2973 *vit-2(crg9070[vit-2::gfp] X;qxEx7587[myo-3p::mCherry + unc-76]*, RB2365 *vit-2(ok3211)* X, MQD2883 *vit-1(hq531) vit-2(ok3211)* X, MQD2884 *vit-1(hq532) vit-2(ok3211)* X, MQD2885 *vit-1(hq533) vit-2(ok3211)* X, and VC988 *ceh-60(ok1485)* X.

Worm strain construction

The CRISPR method for editing the *C. elegans* genome has been fully developed and described before [29]. We thus used CRISPR and separately knocked *mCherry* into the C-terminus of *vit-1*, *vit-3*, and *vit-6* in a BCN9071 *vit-2(crg9070[vit-2::gfp])* background, and knocked out *vit-1* in an RB2365 *vit-2(ok3211)* background. The pDD162 plasmid (Addgene, 47549) of Cas9-sgRNA with no target sequence is available as a commercial product. Two target sequences of sgRNA were designed for every knock-in or knock-out strain. The eight target sequences are shown in Supplementary Table S3.

Homologous repair templates for *mCherry* KI strains were inserted in the vector 95.77-M5. The sequences of the homologous templates are shown in supplementary files (Supplementary files S1–3). The DNA sequences of *vit-1* mutants are shown in supplementary files (Supplementary files S4–6). The pRF4 plasmid, which encodes ROL-6 as a marker for selection, was co-injected. The solution for microinjection contained two Cas9-sgRNA plasmids, the pRF4 plasmid and, if necessary, the plasmid containing homologous repair templates. The final concentration of each plasmid was 50 ng/μL. The primers designed for genotyping are shown in Supplementary Table S4.

Antibodies

The rat polyclonal anti-VIT-2 antibody (diluted to 1:100 for immuno-EM labeling, to 1:100 for immuno-fluorescent staining, and to 1:6,000 for Western blot assay) was kindly provided by Dr. Xiao-Chen Wang (Institute of Biophysics, Chinese Academy of Sciences, Beijing, China). The epitope of the antibody is recombinant protein VIT-2 (83–620 amino acids)::6×His [28]. The mouse monoclonal anti-GFP antibody was a commercial product from Roche (11814460001, diluted to 1:50 for immuno-EM labeling and to 1:3000 for Western blot assay). The goat anti-rat conjugated with 10-nm colloidal gold (Sigma, G7035), the goat anti-mouse conjugated with 6-nm colloidal gold (AURION, 106.022), the donkey anti-mouse conjugated with 12-nm colloidal gold (Jackson ImmunoResearch, 715-205-150), the goat anti-rat conjugated with Alexa Fluor® 488 (Thermo, A-11006), and the goat anti-mouse conjugated with Alexa Fluor® 594 (Jackson ImmunoResearch, 115-585-003) were available as commercial products. The secondary antibodies used in the western blot assay were goat anti-mouse (Sigma, AP124) and goat anti-rat (CW bio, 01340/40126).

Western blot assay and Coomassie staining

Forty hermaphrodites at AD 1 were put into 20 μL M9 buffer and frozen in liquid nitrogen as soon as possible. To homogenize the worms, 5 μL 5× SDS sample buffer was added and the samples were boiled at 100°C for 10 min. After that, the samples were stirred gently using a pipette and then centrifuged at 13,000 rpm at 4°C for 10 min. The supernatant was loaded on a polyacrylamide gel for electrophoresis (PAGE) (80 V, 40 min; 120 V, 110 min). Proteins in the SDS–PAGE gel were transferred to a PVDF membrane at 100 V for 120 min. The anti-VIT-2 antibody and anti-GFP antibody were diluted to 1:6000 and 1:3000, respectively, in blocking solution (5% de-fat milk in TBST) for Western blot assay. The anti-rat and anti-mouse antibodies were diluted to 1:5000 and 1:3000, respectively, in the blocking solution. All original images of Western blot results are displayed in blot transparency in supplementary files.

After electrophoresis, the polyacrylamide gel was placed in the transfer buffer to remove impurities. The polyacrylamide gel was then stained in Coomassie staining solution (0.1% Coomassie Blue R-250, 50% methanol (MeOH), 10% acetic acid (HOAc), 39.9% H_2O) for 4 h. The gel was washed by the destaining solution (50% MeOH, 10% HOAc, 40% H_2O) before being photographed.

Immuno-fluorescent staining

The immuno-fluorescent staining was conducted by adapting the protocol of Duerr [62]. AD 2 worms were collected by centrifugation at 2000 rpm for 1 min. The worm pellet was dropped onto a poly-lysine (Sigma, P9155) coated glass slide, covered with an uncoated glass side, and placed on dry ice immediately. When frozen, the "sandwich" was split open, and the worm pellet, which stuck to the coated glass slide, was fixed in pre-cooled MeOH (4°C for 2 min) and acetone (4°C for 4 min) before being washed three times with pre-cooled phosphate-buffered saline (PBS) (4°C, pH 7.4), 10 min each time. Then the sample was blocked with 5% BSA for 1 h at room temperature before it was incubated with the primary antibody (the anti-VIT-2 or anti-GFP antibodies were diluted to 1:100 in 1% BSA antibody buffer) overnight at 4°C. After washing with pre-cooled PBS (pH 7.4) three times, 20 min each time, the sample was incubated with the secondary antibody (anti-rat conjugated with Alexa Fluor® 488 or anti-mouse conjugated with Alexa Fluor® 594 with 1:100 dilution) for 4 h at room temperature, and then washed again with pre-cooled PBS (4°C, pH 7.4) for three times, 20 min each time. Lastly, 20 μL 2.5% DAPI (4′-6-diamidino-2-phenylindole) and 100 μL 50% glycerol were added onto the worm sample spot, topped by a coverslip, and sealed off with nail polish.

High-pressure freezing and freeze-substitution

The procedure of high-pressure freezing was explained before [63], but a few conditions were optimized here for the nematode samples. The main steps are shown below. Aluminum carriers (Engineering Office of M. Wohlwend GmbH, 241) were filled with cryoprotectant (20% BSA in M9 buffer). Ten worms of indicated ages (AD 2 and AD 6) were put into a carrier. The carriers were covered with sapphire discs (Engineering Office of M. Wohlwend, 3 mm × 0.16 mm). High-pressure freezing was done using the Wohlwend HPF Compact-01 apparatus.

After high-pressure freezing, every four carriers containing samples were put into a 2-mL polypropylene tube (BIOLOGIX, 81-0204) containing 1 mL substitution solution, including 1% paraformaldehyde, 4% ddH_2O, and 95% acetone. Caps with O-rings (BIOLOGIX, 81-0005) were screwed into the polypropylene tubes.

All steps described above were conducted under liquid nitrogen. Then, the tubes were transferred into a Leica AFS2 freeze-substitution machine for dehydration. The temperature controlling procedure was set as follows: –90°C for 48 h; –90°C to –60°C for 15 h, increase 2°C per hour; –60°C for 8 h; –60°C to –30°C for 15 h, increase 2°C per hour; –30°C for 8 h; and –30°C to 4°C for 17 h, increase 2°C per hour. When the temperature reached 4°C, precooled acetone was used to rinse samples for four times, 15 min each time.

Infiltration and embedding

After dehydration, samples were infiltrated in LR White Resin (London Resin, AGR1281A) at 4°C for 3 days. The worm cakes were taken out from carriers carefully using a pair of needles on a 1-mL syringe under a stereo microscope. Then, every worm cake was transferred into the bottom of a gelatin capsule (Electron Microscopy Sciences, G292-11) that was already filled with 2 drops of LR White Resin containing 0.5% accelerator (London Resin, AGR1283). The capsules were filled with embedding resin and covered with caps to avoid contact with air. Polymerization was performed under UV illumination at 4°C for 24 h. After polymerization, the blocks were stored at –20°C before sectioning.

Sectioning

Blocks were carefully trimmed with a razor under the stereo microscope to make the sample part protrude. Then, a diamond knife (Diatome, DU4530) was used to produce semithin sections (200-nm thick) on the Leica ultramicrotome (UC6, Leica, Germany). Semithin sections were stained with 1% toluidine blue to check whether the anatomic position of the region of interest (ROI) was under the microscope (Chinauop, UB103i). After that, 80-nm ultrathin sections were produced using the diamond knife and collected on nickel grids (Electron Microscopy China, AG50), one side of which was coated with the formvar film made from formvar resin (SPI-Chem, 63148-65-2). Meanwhile, ultrathin sections were also collected on a piece of tape with glow discharge treatment [41]. Finally, nickel grids carrying sections were stored in grid boxes for immuno-labeling.

Immuno-labeling

Immuno-labeling was performed mainly according to Weimer *et al.* [64] with some modifications. In brief, nickel grids carrying worm sections were incubated in 0.05 mol/L glycine in 0.1 mol/L phosphate buffer (PB) (pH 7.4) for 15 min to quench unreacted aldehyde groups in samples. Then, the grids were blocked with 5% BSA in 0.1 mol/L PB (pH 7.4) at room temperature for 1 h, and rinsed three times with 0.1 mol/L PB (pH 7.4). Nickel grids were then incubated with the primary antibody diluted in antibody buffer (1% BSA in 0.1 mol/L PB, pH 7.4) at room temperature for 1 h. To eliminate unspecific labeling, nickel grids were rinsed six times with 0.1 mol/L PB (pH 7.4) for 5 min each time. Then, they were incubated with a colloidal gold-conjugated secondary antibody at room temperature for 1 h. After the antibody solution was removed, the samples were washed nine times with 0.1 mol/L PB (pH 7.4), 5 min per wash. The interaction between primary and secondary antibodies was fixed using 2% glutaraldehyde in 0.1 mol/L PB (pH 7.4) for 5 min, and the nickel grids were rinsed three times with distilled water for 5 min each time. Finally, the nickel grids were stained with uranium acetate and lead citrate.

Conventional EM sample preparation

The conventional EM workflow was as described before [42].

Transmission EM (TEM) and scanning EM (SEM) imaging

For imaging via TEM, nickel grids carrying sections were examined using a Tecnai Spirit 120 microscope (FEI, USA) operating at 120 kV. Images were captured with a MoradeG3 CCD (EMSIS) camera using the RADIUS (EMSIS GmbH) software.

Before SEM imaging, the tapes carrying sections were adhered to SEM Cylinder Specimen Mounts (Electron Microscopy China, DP16232) by carbon conductive double-faced adhesive tape (NISSHIN EM Co. Ltd, Japan), and then the tapes were stained with uranium acetate. The specimen mounts carrying samples were transferred under the SEM (FEI Helios NanoLab 600i) equipped with a CBS detector. Images were acquired by the software xT microscope control (FEI, version 5.2.2.2898) with the SEM parameters set as 2 kV accelerating voltage, 0.69 nA current, and 5 μs dwell time.

Confocal imaging

Fifteen live worms were picked and placed on an agarose pad stuck on a glass slide. Worms were paralyzed with 10 mmol/L levamisole aqueous solution and a coverslip was carefully placed on the top. Images were captured using a fluorescent microscope. Pictures in Supplementary Fig. S4a–c were imaged by SpinSR equipped with a 63× oil-immersion objective (magnification 630×). Images were visualized and processed via the OLYMPUS cellSens Dimension. Pictures in Supplementary Figs. S5c–e and S2 were imaged by a ZEISS LSM 880 microscope equipped with a 63× oil-immersion objective (magnification 630×). Pictures were visualized with the software Axio Vision Rel. 4.7. Pictures in Figs. 2 and 7; Supplementary Figs. S1d–g, S3a–g, and S5a–l′, and images used for quantification were captured using a spinning-disk microscope (UltraVIEW VOX; PerkinElmer) equipped with a 63× oil-immersion objective (magnification 630×). Pictures were visualized with the Volocity® Demo 6.3 software (PerkinElmer).

Quantification of colocalization between VITs

The imaging data for quantification were preprocessed using the Volocity® Demo 6.3 software. For each original image, the brightness of the green fluorescence and that of the red were adjusted to similar levels, respectively, and at the same time, it was made sure that the background remained dark for both the green and the red fluorescence, such as the images in Supplementary Fig. S1d–g. The adjustment was applied to the entire image and was typically between 1× and 2.5× for either channel. The preprocessed images were saved as .jpg files and further analyzed using the ImageJ software. Three rectangular frames of 60–200 μm^2 were randomly placed on a fluorescent image of the intestine, pseudocoelom, oocytes, or embryos (Supplementary Fig. S1d–h). Each frame defined an ROI. Within an ROI, each non-blue-fluorescent punctum (for the intestine and the pseudocoelom) or pixel (for oocytes and embryos) was classified based on its hue value as GFP only (71–90), mCherry only (1–14), or GFP + mCherry (i.e., colocalized, 15–70). A total of 10–70 images of 10–31 worms were quantified for each category. The ratio of colocalization was calculated as the number of colocalized puncta or pixels divided by the total number of vesicles or pixels for each ROI. The hue value 15–70 was used to define the GFP + mCherry ROIs to accommodate the varying intensities of GFP and mCherry in different tissues.

Criteria for annotation of EM images

In general, the criteria for defining an EM subcellular structure are based on the shape, electron density, membrane structure,

size, distribution, and some identical characteristics. Lipid droplets had a lipid monolayer on the outside and uniformly low electron density across, and their size was 1–2 μm in diameter (Supplementary Fig. S6a–d). These characteristics were in keeping with a previous report [65]. ER in the intestine looked like beads (Supplementary Fig. S6e–g) or ribbons (Fig. 4a and b; Supplementary Fig. S6h-i) was decorated with ribosomes. Mitochondria were rounded, oval, and irregular in shape as they can undergo fission or fusion (Supplementary Fig. S6e–l). The most identifiable characteristics of mitochondria were the cristae and the double membrane structures (Supplementary Fig. S6j). In general, mitochondria were smaller than lipid droplets; the minor axis of the mitochondria was 300–500 nm, and the major axis was one to several micrometers depending on where the mitochondria were sectioned. In immuno-EM images, mitochondrial membrane structures were not preserved well, and most of their cristae were nearly invisible (Supplementary Fig. S6c, d, g, h, k, and l). Under this circumstance, the varied profile, higher-electron density textures, and a minor axis of 300–500 nm in diameter were the major criteria for the annotation of mitochondria.

EM image analysis

EM data were quantified using the ImageJ software. The pixel size of the TEM images was calibrated using a standard sample (diffraction grating replica with latex spheres, TED PELLA, INC, 673) at different magnifications. The values are shown in Supplementary Table S5. The quantitative data were analyzed by GraphPad Prism 8.4.3.

Supplementary data

Supplementary material is available at *Life Metabolism* online.

Acknowledgements

We thank Dr. Xiao-Chen Wang from the Institute of Biophysics, Chinese Academy of Science for providing the anti-VIT-2 antibody; Drs. Cheng-Gang Zhou and Bin Liang, both from Yunnan University, for providing the *ceh-60* mutant, the *vit-2* mutant, and the *vit-2::gfp* knock-in worm strains; and the *Caenorhabditis* Genetics Center, which is supported by the NIH Office of Infrastructure Programs (P40 OD010440), for providing the WT N2 strain. We thank Drs. Wan-Zhong He and Zhao-Di Jiang from the National Institute of Biological Sciences (NIBS), Beijing for their technical guidance in EM sample preparation. We thank Dr. Jian-Guo Zhang, Dr. Gang Ji, and Can Peng from the Institute of Biophysics, Chinese Academy of Science for their guidance in EM imaging. We are grateful to Dr. John Hugh Snyder for the critical reading and editing of this manuscript.

Author contributions

Chao Zhai (Data curation [Equal], Formal analysis [Lead], Investigation [Equal], Methodology [Equal], Project administration [Lead], Supervision [Equal], Validation [Equal], Visualization [Equal], Writing—original draft [Equal], Writing—review & editing [Equal]), Nan Zhang (Data curation [Supporting], Formal analysis [Supporting], Investigation [Supporting], Software [Supporting], Validation [Supporting], Visualization [Supporting], Writing—original draft [Supporting]), Xi-Xia Li (Funding acquisition [Supporting], Investigation [Supporting], Project administration [Supporting], Resources [Supporting], Visualization [Supporting]), Xue-Ke Tan (Investigation [Supporting], Methodology [Supporting], Visualization [Supporting]), Fei Sun (Funding acquisition [Equal], Investigation [Supporting], Methodology [Supporting], Project administration [Supporting], Resources [Lead], Software [Supporting], Supervision [Equal], Writing—review & editing [Equal]), and Meng-Qiu Dong (Funding acquisition [Lead], Investigation [Lead], Methodology [Equal], Project administration [Equal], Supervision [Equal], Writing—original draft [Lead], Writing—review & editing [Lead]).

Conflict of interest

M.Q.D. holds the position of Editorial Board Member for *Life Metabolism* and was blinded from reviewing or making decisions for the manuscript. The other authors declare that no conflict of interest exists.

Funding

This work was funded by the National Natural Science Foundation of China (NSFC-ISF 32061143020 to M.Q.D., 31925026 to F.S., and 31501160 to X.X.L.), the Ministry of Science and Technology of the People's Republic of China (institutional grants to NIBS, Beijing, a fund of the National High-Level Talents Special Support Program to M.Q.D.), and Beijing Municipal Science and Technology Commission (institutional grants to NIBS, Beijing and a fund for cultivation and development of innovation base to M.Q.D.).

Ethics approval

All animal protocols were approved by the Institutional Animal Care and Use Committee of National Institute of Biological Sciences, Beijing, China.

Data availability

The authors confirm that all the data supporting the findings of this study are available within the supplementary material and corresponding authors.

References

1. Wu LT, Hui JHL, Chu KH. Origin and evolution of yolk proteins: expansion and functional diversification of large lipid transfer protein superfamily. *Biol Reprod* 2013;**88**:102.
2. Smolenaars MM, Madsen O, Rodenburg KW *et al*. Molecular diversity and evolution of the large lipid transfer protein superfamily. *J Lipid Res* 2007;**48**:489–502.
3. Anderson TA, Levitt DG, Banaszak LJ. The structural basis of lipid interactions in lipovitellin, a soluble lipoprotein. *Structure* 1998;**6**:895–909.
4. Du X, Wang X, Wang S *et al*. Functional characterization of vitellogenin_N domain, domain of unknown function 1943, and von Willebrand factor type D domain in vitellogenin of the non-bilaterian coral *Euphyllia ancora*: implications for emergence of immune activity of vitellogenin in basal metazoan. *Dev Comp Immunol* 2017;**67**:485–94.
5. Li H, Zhang S. Functions of vitellogenin in eggs. *Results Probl Cell Differ* 2017;**63**:389–401.
6. Grant B, Hirsh D. Receptor-mediated endocytosis in the *Caenorhabditis elegans* oocyte. *Mol Biol Cell* 1999;**10**:4311–26.
7. Perez MF, Lehner B. Vitellogenins-yolk gene function and regulation in *Caenorhabditis elegans*. *Front Physiol* 2019;**10**:1067.
8. Sharrock WJ. Cleavage of two yolk proteins from a precursor in *Caenorhabditis elegans*. *J Mol Biol* 1984;**174**:419–31.

9. Sharrock W, Sutherlin ME, Leske K *et al*. Two distinct yolk lipoprotein complexes from *Caenorhabditis elegans*. *J Biol Chem* 1990;**265**:14422–31.
10. Sharrock WJ. Yolk proteins of *Caenorhabditis elegans*. *Dev Biol* 1983;**96**:182–8.
11. Ezcurra M, Benedetto A, Sornda T *et al*. *C. elegans* eats its own intestine to make yolk leading to multiple senescent pathologies. *Curr Biol* 2018;**28**:2544–56.e5.
12. Kimble J, Sharrock WJ. Tissue-specific synthesis of yolk proteins in *Caenorhabditis elegans*. *Dev Biol* 1983;**96**:189–96.
13. Dowen RH. CEH-60/PBX and UNC-62/MEIS coordinate a metabolic switch that supports reproduction in *C. elegans*. *Dev Cell* 2019;**49**:235–50.e7.
14. Van de Walle P, Geens E, Baggerman G *et al*. CEH-60/PBX regulates vitellogenesis and cuticle permeability through intestinal interaction with UNC-62/MEIS in *Caenorhabditis elegans*. *PLoS Biol* 2019;**17**:e3000499.
15. Van Rompay L, Borghgraef C, Beets I *et al*. New genetic regulators question relevance of abundant yolk protein production in *C. elegans*. *Sci Rep* 2015;**5**:16381.
16. Hall DH, Winfrey VP, Blaeuer G *et al*. Ultrastructural features of the adult hermaphrodite gonad of *Caenorhabditis elegans*: relations between the germ line and soma. *Dev Biol* 1999;**212**:101–23.
17. Borgonie G, van Driessche E, Link CD *et al*. Internal lectin binding patterns in the nematodes *Caenorhabditis elegans*, *Panagrolaimus superbus* and *Acrobeloides maximus*. *Fundam Appl Nematol* 1997;**20**:173–86.
18. Britton C, Murray L. Cathepsin L protease (CPL-1) is essential for yolk processing during embryogenesis in *Caenorhabditis elegans*. *J Cell Sci* 2004;**117**:5133–43.
19. Paupard MC, Miller A, Grant B *et al*. Immuno-EM localization of GFP-tagged yolk proteins in *C. elegans* using microwave fixation. *J Histochem Cytochem* 2001;**49**:949–56.
20. Kern CC, Townsend S, Salzmann A *et al*. *C. elegans* feed yolk to their young in a form of primitive lactation. *Nat Commun* 2021;**12**:5801.
21. Murphy CT, McCarroll SA, Bargmann CI *et al*. Genes that act downstream of DAF-16 to influence the lifespan of *Caenorhabditis elegans*. *Nature* 2003;**424**:277–83.
22. Seah NE, de Magalhaes Filho CD, Petrashen AP *et al*. Autophagy-mediated longevity is modulated by lipoprotein biogenesis. *Autophagy* 2016;**12**:261–72.
23. Sornda T, Ezcurra M, Kern C *et al*. Production of YP170 vitellogenins promotes intestinal senescence in *Caenorhabditis elegans*. *J Gerontol A Biol Sci Med Sci* 2019;**74**:1180–8.
24. Wang H, Zhao Y, Ezcurra M *et al*. A parthenogenetic quasi-program causes teratoma-like tumors during aging in wild-type *C. elegans*. *NPJ Aging Mech Dis* 2018;**4**:6.
25. Lemieux G, Ashrafi K. Insights and challenges in using *C. elegans* for investigation of fat metabolism. *Crit Rev Biochem Mol Biol* 2014;**50**:69–84.
26. Wolkow CA, Hall DH. The dauer intestine. In *WormAtlas*; Cold Spring Harbor: New York, 2013.
27. Herndon LA, Schmeissner PJ, Dudaronek JM *et al*. Stochastic and genetic factors influence tissue-specific decline in ageing *C. elegans*. *Nature* 2002;**419**:808–14.
28. Liu B, Du H, Rutkowski R *et al*. LAAT-1 is the lysosomal lysine/arginine transporter that maintains amino acid homeostasis. *Science* 2012;**337**:351–4.
29. Dickinson DJ, Ward JD, Reiner DJ *et al*. Engineering the *Caenorhabditis elegans* genome using Cas9-triggered homologous recombination. *Nat Methods* 2013;**10**:1028–34.
30. Clokey GV, Jacobson LA. The autofluorescent "lipofuscin granules" in the intestinal cells of *Caenorhabditis elegans* are secondary lysosomes. *Mech Ageing Dev* 1986;**35**:79–94.
31. Coburn C, Gems D. The mysterious case of the *C. elegans* gut granule: death fluorescence, anthranilic acid and the kynurenine pathway. *Front Genet* 2013;**4**:151.
32. Coburn C, Allman E, Mahanti P *et al*. Anthranilate fluorescence marks a calcium-propagated necrotic wave that promotes organismal death in *C. elegans*. *PLoS Biol* 2013;**11**:e1001613.
33. Hermann GJ, Schroeder LK, Hieb CA *et al*. Genetic analysis of lysosomal trafficking in *Caenorhabditis elegans*. *Mol Biol Cell* 2005;**16**:3273–88.
34. Teufel F, Almagro Armenteros JJ, Johansen AR *et al*. SignalP 6.0 predicts all five types of signal peptides using protein language models. *Nat Biotechnol* 2022;**40**:1023–5.
35. Balklava Z, Pant S, Fares H *et al*. Genome-wide analysis identifies a general requirement for polarity proteins in endocytic traffic. *Nat Cell Biol* 2007;**9**:1066–73.
36. Saegusa K, Sato M, Morooka N *et al*. SFT-4/Surf4 control ER export of soluble cargo proteins and participate in ER exit site organization. *J Cell Biol* 2018;**217**:2073–85.
37. Bruce A, Alexander J, Julian L *et al.*, Transport from the ER through the Golgi apparatus. In *Molecular Biology of the Cell*; Garland Science: New York, 2002.
38. Herbener GH, Bendayan M, Feldhoff RC. The intracellular pathway of vitellogenin secretion in the frog hepatocyte as revealed by protein A-gold immunocytochemistry. *J Histochem Cytochem* 1984;**32**:697–704.
39. Reading BJ, Sullivan CV, Schilling J, Vitellogenesis in fishes. In: *Reference Module in Life Sciences*; Elsevier, 2017.
40. Gomez-Navarro N, Miller E. Protein sorting at the ER–Golgi interface. *J Cell Biol* 2016;**215**:769–78.
41. Li X, Ji G, Chen X *et al*. Large scale three-dimensional reconstruction of an entire *Caenorhabditis elegans* larva using AutoCUTS-SEM. *J Struct Biol* 2017;**200**:87–96.
42. Zhai C, Zhang N, Li XX *et al*. Fusion and expansion of vitellogenin vesicles during *Caenorhabditis elegans* intestinal senescence. *Aging Cell* 2022;**21**:e13719.
43. Tan D, Li Q, Zhang MJ *et al*. Trifunctional cross-linker for mapping protein-protein interaction networks and comparing protein conformational states. *eLife* 2016;**5**:e12509.
44. Fagotto F. Regulation of yolk degradation, or how to make sleepy lysosomes. *J Cell Sci* 1995;**108**:3645–7.
45. Chen Y, Scarcelli V, Legouis R. Approaches for studying autophagy in *Caenorhabditis elegans*. *Cells* 2017;**6**:27.
46. Costantini LM, Baloban M, Markwardt ML *et al*. A palette of fluorescent proteins optimized for diverse cellular environments. *Nat Commun* 2015;**6**:7670.
47. Costantini LM, Snapp EL. Fluorescent proteins in cellular organelles: serious pitfalls and some solutions. *DNA Cell Biol* 2013;**32**:622–7.
48. Doherty GP, Bailey K, Lewis PJ. Stage-specific fluorescence intensity of GFP and mCherry during sporulation in *Bacillus Subtilis*. *BMC Res Notes* 2010;**3**:303.
49. Katayama H, Yamamoto A, Mizushima N *et al*. GFP-like proteins stably accumulate in lysosomes. *Cell Struct Funct* 2008;**33**:1–12.
50. Snapp E. Design and use of fluorescent fusion proteins in cell biology. *Curr Protoc Cell Biol* 2005;**Chapter 21**:21.4.1–21.4.13.
51. Roth Z, Yehezkel G, Khalaila I. Identification and quantification of protein glycosylation. *J Carbohydr Chem* 2012;**2012**:640923.
52. Fu J, Gao J, Liang Z *et al*. PDI-regulated disulfide bond formation in protein folding and biomolecular assembly. *Molecules* 2020;**26**:171.

53. Hussain MM, Shi J, Dreizen P. Microsomal triglyceride transfer protein and its role in apoB-lipoprotein assembly. *J Lipid Res* 2003;**44**:22–32.
54. Li WJ, Wang CW, Tao L *et al*. Insulin signaling regulates longevity through protein phosphorylation in *Caenorhabditis elegans*. *Nat Commun* 2021;**12**:4568.
55. Lints R, Hall DH, Reproductive system, somatic gonad. In: *WormAtlas*; Cold Spring Harbor: New York, 2009.
56. Geens E, Van de Walle P, Caroti F *et al*. Yolk-deprived *Caenorhabditis elegans* secure brood size at the expense of competitive fitness. *Life Sci Alliance* 2023;**6**:e202201675.
57. Borgonie G, Claeys M, Waele DD *et al*. Ultrastructure of the intestine of the bacteriophagous nematodes *Caenorhabditis elegans*, *Panagrolaimus superbus* and *Acrobeloides maximus*. *Fundam Appl Nematol* 1995;**18**:123–34.
58. Turek M, Banasiak K, Piechota M *et al*. Muscle-derived exophers promote reproductive fitness. *EMBO Rep* 2021;**22**:e52071.
59. Blazie SM, Babb C, Wilky H *et al*. Comparative RNA-Seq analysis reveals pervasive tissue-specific alternative polyadenylation in *Caenorhabditis elegans* intestine and muscles. *BMC Biol* 2015;**13**:4.
60. Kaletsky R, Yao V, Williams A *et al*. Transcriptome analysis of adult *Caenorhabditis elegans* cells reveals tissue-specific gene and isoform expression. *PLoS Genet* 2018;**14**:e1007559.
61. Wang X, Jiang Q, Song Y *et al*. Ageing induces tissue-specific transcriptomic changes in *Caenorhabditis elegans*. *EMBO J* 2022;**41**:e109633.
62. Duerr JS. Antibody staining in *C. elegans* using "Freeze-Cracking". *J Vis Exp* 2013;**80**:e50664.
63. Jiang Z, Jin X, Li Y *et al*. Genetically encoded tags for direct synthesis of EM-visible gold nanoparticles in cells. *Nat Methods* 2020;**17**:937–46.
64. Weimer RM, Preservation of *C. elegans* tissue via High-Pressure Freezing and Freeze-Substitution for ultrastructural analysis and immunocytochemistry. In: Strange K (ed.), *C. elegans: Methods and Applications*. Totowa, NJ: Humana Press, 2006, 203–21.
65. Zhang SO, Trimble R, Guo F *et al*. Lipid droplets as ubiquitous fat storage organelles in *C. elegans*. *BMC Cell Biol* 2010;**11**:96.